Nanoscale

PAPER

View Article Online
View Journal | View Issue

Check for updates

Cite this: *Nanoscale*, 2024, **16**, 9406

A metal–organic cage-derived cascade antioxidant nanozyme to mitigate renal ischemia-reperfusion injury†

Cheng Huang,‡[a,b] Yucen Deng,‡[b] Rongze Ma,‡[b] Hucheng Ge,[a] Fuzhong Gong,*[a] Jinghui Yang,*[c] Xinyuan Zhu[b] and Youfu Wang*[b]

Received 22nd February 2024,
Accepted 4th April 2024

DOI: 10.1039/d4nr00742e

rsc.li/nanoscale

In the field of contemporary medicine, inflammation has emerged as a significant concern in global public health. Among the current anti-inflammatory strategies, nanozymes possess distinctive advantages and demonstrate unexpected efficacy in combating inflammation. However, the indeterminate structures and limited enzyme-like activity exhibited by most developed nanozymes impede their clinical translation and therapeutic effectiveness. In this paper, we developed a nanozyme derived from a well-defined metal–organic cage (MOC). The oxidized MOC (MOC-O), containing pyridine nitrogen oxide moieties, exhibited effective cascade superoxide dismutase (SOD) and catalase (CAT)-like activities for scavenging reactive oxygen species (ROS). This ROS scavenging ability was confirmed through flow cytometry analysis using DCFH-DA in a hypoxia/reoxygenation (H/R) model, where MOC-O significantly alleviated oxidative stress. Furthermore, the administration of MOC-O resulted in preserved renal function during renal ischemia-reperfusion (I/R) injury due to downregulated oxidative stress levels and reduced cell apoptosis.

Published on 04 april 2024. Downloaded on 4-6-2026 02:26:34.

1. Introduction

The kidneys, as vital organs in our body, play a crucial role in maintaining overall health. They are responsible for filtering blood, regulating electrolyte levels, and producing hormones. Nonetheless, these bean-shaped organs are quite susceptible to various stressful conditions, particularly I/R injury, due to their high oxygen demand.[1,2] I/R injury is a common cause of kidney damage, often resulting from medical procedures such as kidney transplantation. This injury occurs when the blood supply to the kidneys is temporarily blocked, resulting in a lack of oxygen and nutrients. Once blood flow is restored, ROS levels increase in the kidneys and pool at the site of injury, which can further damage the already damaged tissues and lead to irreversible kidney failure or kidney fibrosis.[1,3] Thus, the regulation of ROS plays a crucial role in managing I/R injury.

Antioxidant enzymes with highly specific and efficient catalytic activity are the primary mediators for regulating ROS in a biological system.[4] Antioxidant enzymes, such as peroxidase, SOD, and CAT, play a pivotal role in mitigating oxidative stress and safeguarding cellular integrity.[5–7] However, they are not sufficient to provide optimal protection at high concentrations of oxidants.[8] Natural enzymes also face some challenges such as unstable structures, susceptibility to inactivation, complex preparation, high cost, and difficulty in long-term preservation. These limitations of natural enzymes restrict their further development. To solve these problems, nanozymes are promoted to replace natural enzymes.[5,6,9–12] Nanozymes possessing distinctive physical, chemical, and biological properties inherent to nanomaterials along with enzyme-like catalytic activity are a subject of continuous exploration and research.[13–16] Compared with natural enzymes, nanozymes have the advantages of easy preparation, high stability and low cost, which makes nanozymes continue to develop rapidly, and have been widely used in biomedicine, environmental protection, energy supply and other fields.[9,10] After over a decade of extensive development, the repertoire of nanozymes has progressively expanded to encompass key enzymes such as SOD, glutathione peroxidase, CAT, and phosphatases, among others.[10] However, nanozymes still encounter various limitations, including indeterminate structures, unvarying enzyme activity, and diminished biosafety.[5,6,11] Therefore, it is imperative for researchers to prioritize the development of structurally precise and low-toxic

[a]*School of Chemistry and Chemical Engineering, Guangxi University, Nanning 530004, China. E-mail: fzgong@gxu.edu.cn*
[b]*School of Chemistry and Chemical Engineering, Shanghai Jiao Tong University, Shanghai 200240, China. E-mail: wyfown@sjtu.edu.cn*
[c]*Department of Organ Transplantation, Shanghai Changzheng Hospital, Naval Medical University, Shanghai 200003, China. E-mail: yjh@smmu.edu.cn*
†Electronic supplementary information (ESI) available. See DOI: https://doi.org/10.1039/d4nr00742e
‡These authors contributed equally to this work.

This journal is © The Royal Society of Chemistry 2024

Published on 04 april 2024. Downloaded on 4-6-2026 02:26:34.

nanozymes with multiple activities, aiming to advance their clinical applications in disease treatment.[5,12,17]

MOCs are innovative porous nanomaterials featuring precise and customizable nanostructures at the atomic level, and are synthesized by coordinating metal clusters or ions with organic ligands through coordination bonds. These materials exhibit exceptional properties and functionalities, making them highly versatile for a wide range of applications.[11,12,18–20] The stable, adjustable, and nanoscale structures, porousness, and biocompatibility of MOCs confer significant advantages and potential as nanozymes.[21] However, at this stage, limited research has been conducted on the utilization of MOCs as nanozymes with antioxidant properties. We believe that the multifunctional nature of MOCs as antioxidant nanozymes makes them highly advantageous and poised to garner increased attention in the future.[22–24]

Herein, we aim to fabricate an antioxidant nanozyme based on a well-defined MOC. It is worth noting that pyridine nitrogen oxides have been proven effective as reducing agents for scavenging ROS.[25,26] Initially, MOCs constructed directly from ligands containing pyridine nitrogen oxide moieties were considered. However, our attempts to obtain the desired MOC using the related ligand were unsuccessful. Therefore, we prepared an MOC with bipyridyl ligands and subsequently oxidized them to form MOC-O containing pyridine nitrogen oxides through post-synthetic modification using *m*-chloroperbenzoic acid, as depicted in Scheme 1A. After the structural characterization of MOC-O, we analyzed the performance of the antioxidant nanozyme. Surprisingly, MOC-O exhibits both SOD-like activity, by converting $^{\bullet}O_2^-$ to H_2O_2 and O_2, and CAT-like activity, by converting H_2O_2 to H_2O and O_2 (Scheme 1B). This ROS scavenging ability was further confirmed through flow cytometry analysis using DCFH-DA in an H/R model, where MOC-O significantly mitigated oxidative stress. Moreover, the administration of MOC-O resulted in preserved renal function during renal I/R injury due to downregulated oxidative stress levels and reduced cell apoptosis (Scheme 1C).

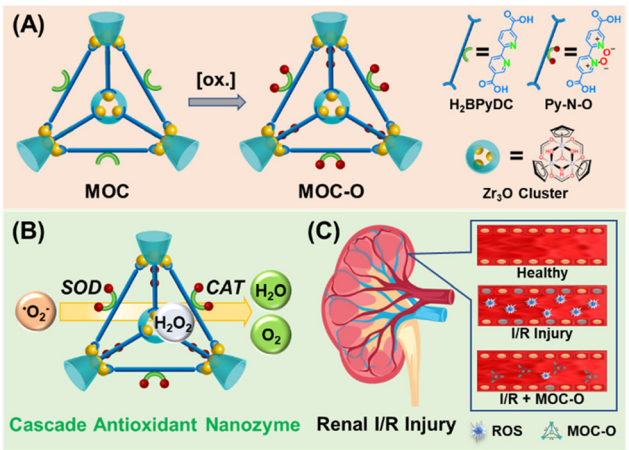

Scheme 1 Fabrication, cascade enzyme-like activities, and therapeutic efficacy of the MOC-O cascade nanozyme for renal I/R injury.

2. Results and discussion

2.1 Structural characterization of the MOC-O nanozyme

A zirconium-based tetrahedral MOC was prepared through a solvothermal method from 2,2′-bipyridine-5,5′-dicarboxylic acid (H_2BPyDC) and bis(cyclopentadienyl)zirconium dichloride (Cp_2ZrCl_2, Cp = η^5-C_5H_5), according to the previous reports.[27,28] Then the MOC was oxidized to MOC-O utilizing *m*-chloroperbenzoic acid (ESI†).[29,30] The structural confirmation of the obtained MOC-O was accomplished through nuclear magnetic resonance (NMR), mass spectrometry, and Fourier transform infrared (FT-IR) spectroscopy.

The ^{1}H-NMR spectra of the MOC and MOC-O in DMOS-d_6 were compared, revealing nearly identical peak profiles. The peaks of MOC-O, however, exhibited a shift towards a higher field attributed to the electronic effect arising from the presence of the pyridine nitrogen oxide moiety. Specifically, the characteristic bipyridine peaks at 9.02, 8.26, and 8.10 ppm in the MOC were shifted to 8.95, 8.15, and 8.05 ppm in MOC-O, respectively. Additionally, the Cp peak also experienced a shift from 6.72 to 6.55 ppm (Fig. 1A, Fig. S1 and S2 in the ESI†). This result represents the preliminary verification of the successful synthesis of MOC-O. The structure of MOC-O was further confirmed through matrix-assisted laser desorption ionization time-of-flight (MALDI-TOF) mass spectrometry. The three peaks observed at approximately 3643, 3691, and 3771 correspond to the oxidation of the MOC at 3, 6, and 11 sites, respectively (Fig. 1B, Fig. S3 in the ESI†), indicating that both pyridinyl moieties within one ligand in H_2BPyDC can be oxidized. Additionally, FT-IR spectroscopy was employed to confirm the structure of MOC-O. The spectra of both the MOC and MOC-O shared remarkable similarities, with all characteristic peaks of the MOC also observed in the spectrum of MOC-O. Moreover, a distinct peak corresponding to N–O

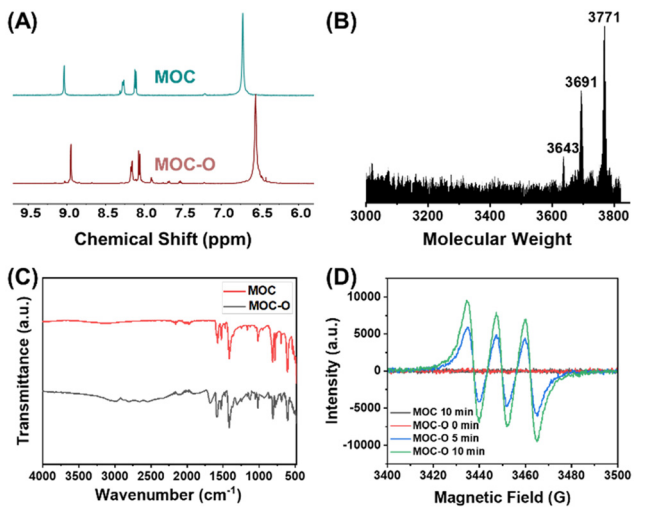

Fig. 1 The structural characterization of MOC and MOC-O nanozymes. (A) The ^{1}H-NMR spectra of the MOC and MOC-O in DMSO-d_6. (B) The MALDI-TOF mass spectrum of MOC-O. (C) The FT-IR spectra of the MOC and MOC-O. (D) The EPR curves of the MOC and MOC-O.

Published on 04 april 2024. Downloaded on 4-6-2026 02:26:34.

appeared at 1300 cm^{-1} in the spectrum of MOC-O (Fig. 1C).[31,32] All aforementioned tests provide evidence for the successful synthesis of well-designed MOC-O.

Electron paramagnetic resonance (EPR) is a technique used to detect unpaired electrons in atoms or molecules and investigate the structural properties of their environment.[33] Pyridine nitrogen oxides can be oxidized using oxidizing agents to generate an intermediate oxidation state, which may further decompose or isomerize into free radicals. Therefore, we performed an EPR test on the MOC and MOC-O. As pyridine nitrogen oxides are absent in the MOC, no EPR signal was detected; however, a strong signal of free radicals was observed in MOC-O, providing further evidence for the synthesis of the desired MOC-O (Fig. 1D).

2.2 *In vitro* SOD- and CAT-like activities of the cascade nanozyme

Due to the intriguing EPR effect exhibited by MOC-O, we further investigated its enzyme-like activities such as those of SOD and CAT. We used the nitrotetrazolium blue chloride (NBT) method for determining SOD-like activity (ESI†).[34,35] Upon exposure to UV irradiation, riboflavin and methionine generate $^{\bullet}O_2^-$, which selectively reduces NBT to form a blue-colored methylhydrazone compound exhibiting maximum absorbance at 560 nm. Nevertheless, the inclusion of either SOD or SOD-mimicking nanozymes led to efficient quenching of $^{\bullet}O_2^-$ radicals, thereby impeding the formation of methylhydrazone. To elucidate the origin of enzyme activity, we employed a commercially available pyridine nitrogen oxide analogue, namely 2,2′-bipyridine-1,1′-dioxide (2,2′-BPDO), as a control group. In comparison with the control group, minimal SOD-like activity was observed in the MOC, whereas both 2,2′-BPDO and MOC-O exhibited remarkable SOD enzyme activity with MOC-O demonstrating superior performance (Fig. 2A). The concentration-dependent SOD-like activity demonstrates an augmented SOD-like activity as the MOC-O concentration increases. Consequently, it can be inferred that the primary origin of SOD-like activity in MOC-O is attributed to pyridine nitrogen oxide moieties (Fig. 2B).

The CAT-like activity of MOC-O was determined at room temperature by quantifying the oxygen generated using a specialized oxygen electrode on a Speedwell Split Dissolved Oxygen Meter (SW9403). It was observed that both the blank and MOC groups exhibited relatively low CAT-like activities; however, in contrast, 2,2′-BPDO and MOC-O groups demonstrated efficient CAT-like activities. Notably, among these groups, the MOC-O group exhibited superior performance, thereby confirming its excellent CAT-like activity (Fig. 2C). Furthermore, the CAT-like activity exhibited a positive correlation with increasing concentrations of MOC-O (Fig. 2D).

2.3 *In vitro* ROS-scavenging ability of MOC-O to protect HK-2 cells

To further investigate the ROS-scavenging activity of MOC-O at the cellular level, a series of tests were conducted. First, 3-(4,5-dimethylthiazol-2-yl)-2,5-diphenyltetrazolium bromide (MTT)

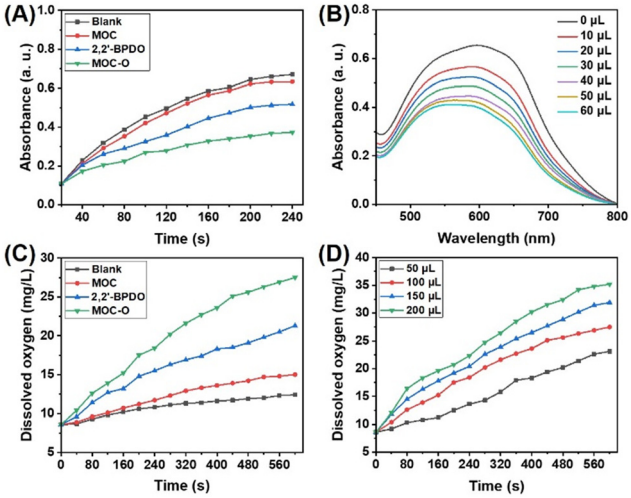

Fig. 2 The antioxidant enzyme-like activities of the MOC-O nanozyme. (A) Temporal variation in the SOD-like activities of the MOC, 2,2′-BPDO, and MOC-O. (B) The relationship between the amount of MOC-O and its SOD-like activity. (C) A comparison of CAT-like activities among the MOC, 2,2′-BPDO, and MOC-O. (D) The impact of the amount of MOC-O on its CAT-like activity.

was employed to assess the cytotoxicity of MOC-O on HK-2 cells (human renal proximal tubule cells) (Fig. 3A). The viability of HK-2 cells remained above 90% across different concen-

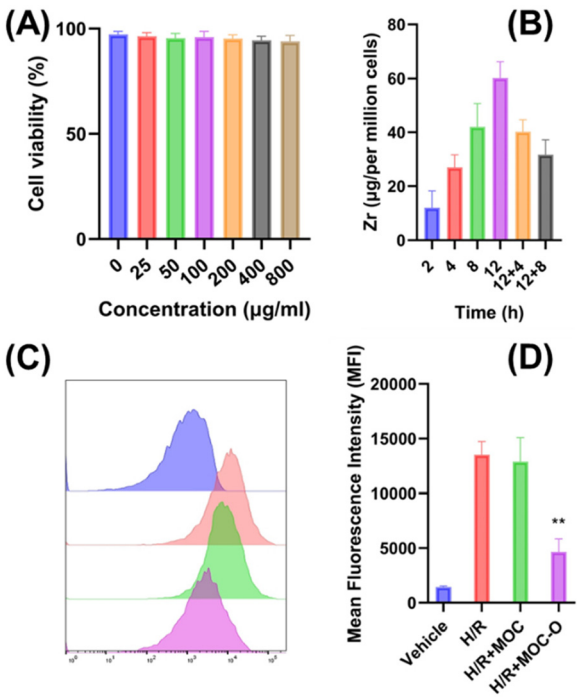

Fig. 3 *In vitro* cytoprotective and ROS-scavenging efficacy of MOC-O. (A) The impact of MOC-O on HK-2 cell viability assessed using the MTT assay. (B) Cellular uptake of MOC-O in HK-2 cells. (C) Flow cytometry analysis and (D) fluorescence intensity measurements performed to evaluate the effects of different treatments on HK-2 cells following H/R.

This journal is © The Royal Society of Chemistry 2024

Published on 04 april 2024. Downloaded on 4-6-2026 02:26:34.

trations of MOC-O solution, indicating its minimal toxic effects and excellent biocompatibility with HK-2 cells. Furthermore, even at a high concentration of MOC-O solution (2 mg ml^{-1}), the hemolysis rate was found to be less than 2%, confirming that MOC-O exhibited no toxicity towards erythrocytes as well (Fig. S4, ESI†).

Inductively coupled plasma mass spectrometry (ICP-MS) was employed to quantify zirconium levels within the cells, enabling investigation of the cellular uptake of MOC-O. The rate of cellular uptake exhibited a linear increase over time until reaching 12 hours, indicating that the uptake process reached saturation and remained stable at this concentration (Fig. 3B). Following the withdrawal of MOC-O, its concentration rapidly declined within the initial 4 hours and subsequently decreased gradually. To investigate intracellular oxidative stress, we employed DCFH-DA, a fluorescent probe that emits a green fluorescence signal upon encountering free radicals. As shown in Fig. 3C and D, H/R treatment significantly augmented the level of free radicals in HK-2 cells, while MOC lacking pyridine *N*-oxides exhibited no discernible impact on reducing free radicals. Conversely, MOC-O demonstrated remarkable efficacy in diminishing the levels of free radicals in HK-2 cells, thereby showcasing its exceptional capacity for scavenging free radicals.

2.4 MOC-O protected against renal I/R injury

To investigate the biocompatibility of MOC-O in major organs including the heart, liver, lungs and kidneys in mice, tissue samples were collected after two days of treatment and subjected to histological analysis using hematoxylin and eosin (H&E) staining.[2,36] As shown in Fig. 4A, all organs from the three groups exhibited uniform organization with no apparent signs of damage. Blood biochemical markers for liver and kidney injury such as alanine aminotransferase (ALT), aspartate aminotransferase (AST), blood urea nitrogen (BUN) and creatinine were measured (Fig. 4B–E). The results indicated that there were no statistically significant differences observed among the three groups with respect to these injury biomarkers, suggesting the absence of any deleterious effects on the mice.

To investigate the protective effect of MOC-O against renal I/R injury, mice in each group were subjected to 30 minutes of ischemia. The kidney tissues of mice in the sham operation group (Sham) exhibited no abnormalities, indicating the absence of evident damage. In contrast, the kidney tissues of mice in both the I/R group and the I/R + MOC group showed noticeable tubular necrosis and significant damage following I/R injury. In contrast, MOC-O-treated mice exhibited a conspicuous absence of tubular fragments following I/R injury and minimal observed kidney damage (Fig. 5A and C). Considering the pivotal roles of cytokines, such as TNF-α, IL-1β, and IL-6, in I/R-induced renal injury, we conducted a comparative analysis of their expression levels among different groups. Intriguingly, mRNA levels for TNF-α, IL-1β, and IL-6 were significantly elevated in both I/R control mice and MOC-treated mice compared to those observed in MOC-O-treated

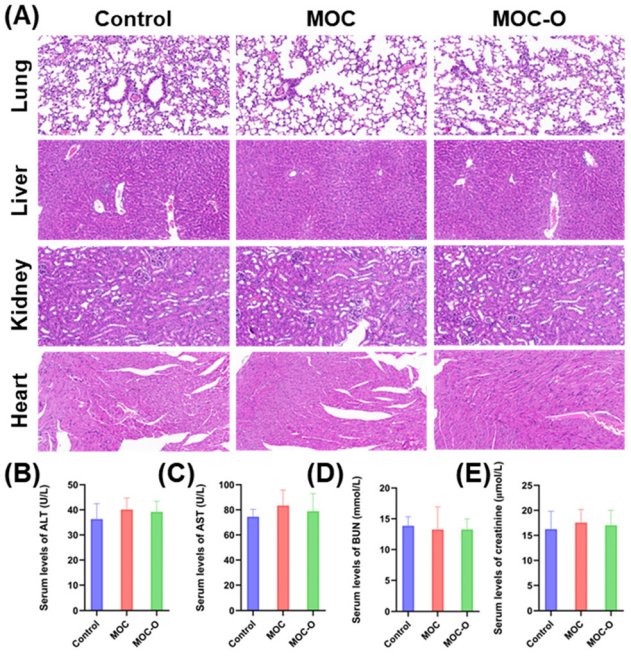

Fig. 4 The evaluation of the biocompatibility of MOC-O. (A) H&E staining of major organs. (B–E) The serum levels of ALT, AST, BUN, and creatinine.

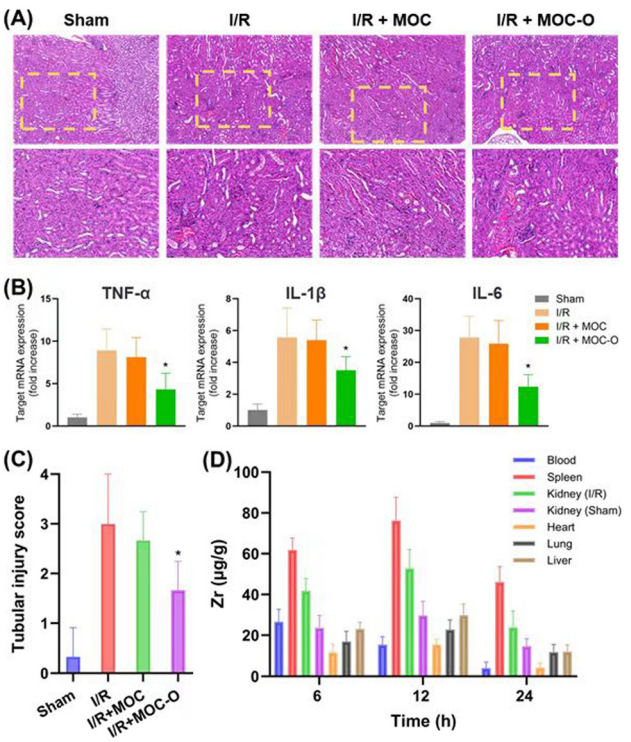

Fig. 5 The renal protection effect and biodistribution of MOC-O. (A) H&E staining of the kidneys at 12 hours post reperfusion (20× and 40× original magnification). (B) The mRNA levels of IL-1β, TNF-α, and IL-6 in renal tissue. (C) Kidney injury measured according to tubular injury scores. (D) Biodistribution of MOC-O in different tissues at various time points.

Published on 04 april 2024. Downloaded on 4-6-2026 02:26:34.

mice (Fig. 5B). These findings provide compelling evidence for the beneficial protective effect exerted by MOC-O against renal I/R-induced damage.

To further elucidate the protective mechanism underlying MOC-O-mediated attenuation of renal I/R injury, we employed ICP-MS to investigate the biodistribution of MOC-O at various time points post-injection. The blood concentration of MOC-O decreased over time at 6 h, 12 h, and 24 h (Fig. 5D). Notably, among the organs examined, the spleen and kidneys exhibited the highest accumulation of MOC-O, while the liver, lungs, and heart showed relatively low levels. Moreover, within the kidney tissue samples collected from both I/R and sham-operated groups, a higher concentration of MOC-O was observed in the kidneys of the I/R group compared to the kidneys of the sham group, demonstrating remarkable ease in traversing the fenestrated endothelium, the glomerular basement membrane junction, and the podocyte slit of the damaged kidneys, showcasing its potency in facilitating the repair and regeneration of renal tissues.

We next investigated whether the observed ROS scavenging capacity *in vitro* could account for the protective effects of MOC-O on assaulted kidneys. Dihydroethidium (DHE) is widely employed as a fluorescence detection probe for ROS, specifically targeting superoxide anions, making it one of the most frequently utilized probes in research studies. As shown in Fig. 6A, the level of ROS induced after reperfusion among different groups was assessed using DHE staining. Compared to the sham group, an increase in ROS levels was observed in the I/R group, strongly suggesting a pivotal role of oxidative stress in the early stage of I/R injury. As expected, treatment with MOC-O effectively scavenged tissue ROS, while MOC exhibited limited capacity for ROS scavenging.

Generally, ROS can function as signaling molecules that initiate the activation of pro-apoptotic pathways in response to various cellular stresses such as I/R injury. However, if the cellular stress is too severe or persists for a prolonged period, the pro-apoptotic pathways activated by ROS become irreversible, leading to cell death and tissue damage. In this study, TUNEL assay was employed to quantify the level of cellular apoptosis in I/R-induced renal damage. Our findings demonstrate a significant reduction in the percentage of TUNEL-positive cells in MOC-O-treated groups compared to the I/R group, indicating a pronounced attenuation of renal apoptosis by MOC-O under assault from I/R (Fig. 6B and C).

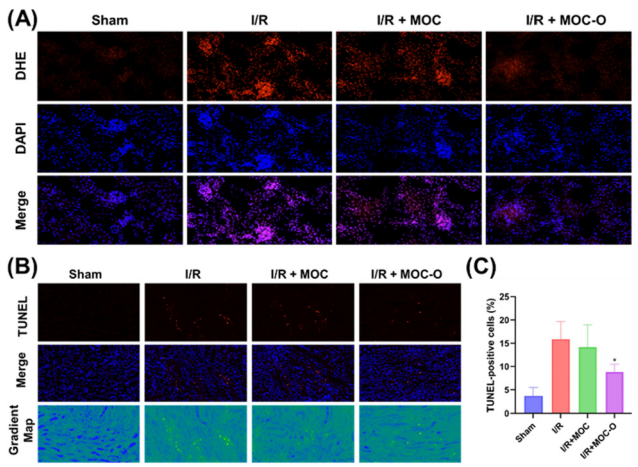

Fig. 6 The ROS-scavenging and anti-apoptosis capabilities of MOC-O. (A) The levels of ROS evaluated using DHE staining. (B) Representative immunofluorescence images of kidney sections stained with TUNEL. (C) The percentage of TUNEL-positive cells.

3. Conclusions

In conclusion, a nanozyme derived from an MOC was constructed with precise structures and exhibited cascade antioxidant activities. Through post-synthesis modification, MOC-O with pyridine nitrogen oxide moieties was obtained and characterized. The presence of pyridine nitrogen oxides enabled effective scavenging of ROS and demonstrated excellent antioxidant capacity. Notably, MOC-O showed cascade nanozyme performance resembling SOD and CAT, primarily attributed to the pyridine nitrogen oxide moieties. Furthermore, MOC-O exhibited favorable biocompatibility and remarkable ROS scavenging capabilities at both cellular and *in vivo* levels. *In vivo* experiments further confirmed the ability of MOC-O to effectively protect against kidney I/R damage and cell apoptosis. Overall, MOC-O represents a novel and efficient cascade antioxidant nanozyme that holds promising prospects for future clinical applications in medicine. Moreover, the simple yet effective method employed for modifying the MOC with redox properties may cater to diverse needs in biomedical research as well as energy and environmental sectors.

Author contributions

Y. W. conceived the idea. C. H., Y. D., and R. M. contributed equally to this work and conducted most of the experiments. H. G. supported the data analysis. X. Z. and F. G. supervised the data analysis. C. H., J. Y., and Y. W. wrote the manuscript. All authors discussed the results and have given approval to the final version of the manuscript.

Conflicts of interest

There are no conflicts to declare.

Acknowledgements

This work was supported by the National Key R&D Program of China (Key Special Project for Marine Environmental Security and Sustainable Development of Coral Reefs 2022-3.5), the Fundamental Research Funds for the Central Universities (YG2023QNA04 and YG2022QN027), and the Shanghai

This journal is © The Royal Society of Chemistry 2024

Published on 04 april 2024. Downloaded on 4-6-2026 02:26:34.

Municipal Health Commission Clinical Research Project (20214Y0521).

All animal experiments were performed in accordance with the guidelines of the National Institute of Health for the Care and Use of Laboratory Animals and approved by the Scientific Investigation Board of Shanghai Changzheng Hospital (No. 2023091501).

References

1 G. Chen, Y. Yu, X. Fu, G. Wang, Z. Wang, X. Wu, J. Ren and Y. Zhao, *J. Colloid Interface Sci.*, 2022, **607**, 1382–1390.
2 J. Kong, R. Zou, R. Chu, N. Hu, J. Liu, Y. Sun, X. Ge, M. Mao, H. Yu and Y. Wang, *ACS Nano*, 2023, **18**, 4140–4158.
3 B. Yang, H. Yao, J. Yang, C. Chen, Y. Guo, H. Fu and J. Shi, *J. Am. Chem. Soc.*, 2022, **144**, 314–330.
4 Y. Huang, C. Liu, F. Pu, Z. Liu, J. Ren and X. Qu, *Chem. Commun.*, 2017, **53**, 3082–3085.
5 A. M. Villalba-Rodríguez, L. Y. Martínez-Zamudio, S. A. H. Martínez, J. A. Rodríguez-Hernández, E. M. Melchor-Martínez, E. A. Flores-Contreras, R. B. González-González and R. Parra-Saldívar, *Top. Catal.*, 2022, **66**, 707–722.
6 J. Wu, X. Wang, Q. Wang, Z. Lou, S. Li, Y. Zhu, L. Qin and H. Wei, *Chem. Soc. Rev.*, 2019, **48**, 1004–1076.
7 R. Radi, *Proc. Natl. Acad. Sci. U. S. A.*, 2018, **115**, 5839–5848.
8 C. A. Ferreira, D. Ni, Z. T. Rosenkrans and W. Cai, *Nano Res.*, 2018, **11**, 4955–4984.
9 Y. Qiu, G. Tan, Y. Fang, S. Liu, Y. Zhou, A. Kumar, M. Trivedi, D. Liu and J. Liu, *New J. Chem.*, 2021, **45**, 20987–21000.
10 Y. Huang, J. Ren and X. Qu, *Chem. Rev.*, 2019, **119**, 4357–4412.
11 N. Ahmad, H. A. Younus, A. H. Chughtai and F. Verpoort, *Chem. Soc. Rev.*, 2015, **44**, 9–25.
12 S. K. Samanta and L. Isaacs, *Coord. Chem. Rev.*, 2020, **410**, 213181.
13 L. Zuo, H. King, M. A. Hossain, F. Farhana, M. M. Kist, R. L. Stratton, J. Chen and H. Shen, *Chem. Biomed. Imaging*, 2023, **1**, 760–766.
14 Y. Kang, C. Li, H. Shi, A. Zhang, C. Huang, C. Zhou and N. Jia, *Chin. J. Chem.*, 2023, **41**, 3189–3196.
15 W. Jiang, Q. Li, R. Zhang, J. Li, Q. Lin, J. Li, X. Zhou, X. Yan and K. Fan, *Nat. Commun.*, 2023, **14**, 8137.
16 Q. Li, T. Wu, O. U. Akakuru, N. Song, W. Liu, W. Jiang and K. Fan, *Adv. Funct. Mater.*, 2023, **33**, 2214826.
17 J. H. Zhang, S. M. Xie, M. Zi and L. M. Yuan, *J. Sep. Sci.*, 2019, **43**, 134–149.
18 D. Sun, X. Feng, X. Zhu, Y. Wang and J. Yang, *Coord. Chem. Rev.*, 2024, **500**, 215546.
19 C. Huang, J. Li, X. Zhu and Y. Wang, *Nanoscale*, 2023, **15**, 19475–19479.
20 X. Ning, P. Yin, L. Zhang, F. Gao, Y. Wang and J. Yang, *New J. Chem.*, 2024, **48**, 6557–6561.
21 G. Liu, M. Zeller, K. Su, J. Pang, Z. Ju, D. Yuan and M. Hong, *Chem. – Eur. J.*, 2016, **22**, 17345–17350.
22 D. Zhang, T. K. Ronson and J. R. Nitschke, *Acc. Chem. Res.*, 2018, **51**, 2423–2436.
23 W.-X. Gao, H.-N. Zhang and G.-X. Jin, *Coord. Chem. Rev.*, 2019, **386**, 69–84.
24 E. M. El-Sayed, Y. D. Yuan, D. Zhao and D. Yuan, *Acc. Chem. Res.*, 2022, **55**, 1546–1560.
25 H. S. Moradi, E. Momenzadeh, M. Asar, S. Iranpour, A. R. Bahrami, M. Bazargan, H. Hassanzadeh, M. M. Matin and M. Mirzaei, *J. Mol. Struct.*, 2022, **1249**, 131584.
26 P. O. Dunstan, *J. Therm. Anal. Calorim.*, 2011, **106**, 327–331.
27 A. Palav, B. Misal, A. Ernolla, V. Parab, P. Waske, D. Khandekar, V. Chaudhary and G. Chaturbhuj, *Org. Process Res. Dev.*, 2018, **23**, 244–251.
28 K. I. Burton, I. Elser, A. E. Waked, T. Wagener, R. J. Andrews, F. Glorius and D. W. Stephan, *Chem. – Eur. J.*, 2021, **27**, 11730–11737.
29 M. Zhou, G. Liu, Z. Ju, K. Su, S. Du, Y. Tan and D. Yuan, *Cryst. Growth Des.*, 2020, **20**, 4127–4134.
30 C. Ji, W. Wang, E.-S. M. El-Sayed, G. Liu, Y. Si, K. Su, Z. Ju, F. Wu and D. Yuan, *Appl. Catal., B*, 2021, **285**, 119782.
31 M. Kumar, M. Srivastava and R. A. Yadav, *Spectrochim. Acta, Part A*, 2013, **111**, 242–251.
32 F. Kang, X. Wang, C. Chen, C.-S. Lee, Y. Han and Q. Zhang, *J. Am. Chem. Soc.*, 2023, **145**, 15465–15472.
33 H. F. V. Victória, D. C. Ferreira, J. B. G. Filho, D. C. S. Martins, M. V. B. Pinheiro, G. d. A. M. Sáfar and K. Krambrock, *Free Radical Biol. Med.*, 2022, **180**, 143–152.
34 Z. Tu, Y. Zhong, H. Hu, D. Shao, R. Haag, M. Schirner, J. Lee, B. Sullenger and K. W. Leong, *Nat. Rev. Mater.*, 2022, **7**, 557–574.
35 L. Zhang, Y. Zhang, Z. Wang, F. Cao, Y. Sang, K. Dong, F. Pu, J. Ren and X. Qu, *Mater. Horiz.*, 2019, **6**, 1682–1687.
36 J. Yang, H. Liu, S. Han, Z. Fu, J. Wang, Y. Chen and L. Wang, *FASEB J.*, 2020, **34**, 12324–12337.